Bifurcation analysis of delay-induced resonances of the El-Niño Southern Oscillation

By Bernd Krauskopf[1] and Jan Sieber[2],

[1]*Department of Mathematics, The University of Auckland, New Zealand*
[2]*College of Engineering, Mathematics and Physical Sciences, University of Exeter, UK*

Models of global climate phenomena of low to intermediate complexity are very useful for providing an understanding at a conceptual level. An important aspect of such models is the presence of a number of feedback loops that feature considerable delay times, usually due to the time it takes to transport energy (for example, in the form of hot/cold air or water) around the globe.

In this paper we demonstrate how one can perform a bifurcation analysis of the behaviour of a periodically-forced system with delay in dependence on key parameters. As an example we consider the El-Niño Southern Oscillation (ENSO), which is a sea surface temperature oscillation on a multi-year scale in the basin of the Pacific Ocean. One can think of ENSO as being generated by an interplay between two feedback effects, one positive and one negative, which act only after some delay that is determined by the speed of transport of sea-surface temperature anomalies across the Pacific. We perform here a case study of a simple delayed-feedback oscillator model for ENSO (introduced by Tziperman *et al*, J. Climate 11 (1998)), which is parametrically forced by annual variation. More specifically, we use numerical bifurcation analysis tools to explore directly regions of delay-induced resonances and other stability boundaries in this delay-differential equation model for ENSO.

1. Introduction

In climate science one finds a hierarchy of increasingly complex mathematical models, all the way from low-dimensional conceptual models in the form of ordinary differential equations (ODE) to global climate models with many millions of unknowns. Our interest here is in models of a low to intermediate complexity, in particular, those that feature delayed feedback mechanisms. The mathematical description of such a system, hence, takes the form of delay differential equations (DDEs). Despite looking similar to ODEs at first sight, DDEs have an infinite-dimensional phase space (that is, space of possible initial conditions), which enables them to describe complex phenomena even with a low number of dependent variables [1]. This type of model arises in other fields of science, for example, in mechanical engineering, in laser physics and in mathematical biology, where one finds communication delays (between optical elements or cells) as well as processing delays; see, for example, [2, 3]. In climate science, on the other hand, delays arise mainly in feedback loops due to the transport of mass or energy from one location on the planet to another. There are models that describe such transport phenomena directly in the form of partial differential equations [4]. However, in some situations it is advantageous to take a more conceptual point of view by considering only the resulting feedback effect itself, which is then subject to a delay due to the associated transport time.

TeX Paper

In this contribution we perform a case study of such a DDE model to demonstrate how tools from bifurcation theory can be brought to bear to understand its behaviour. More specifically, we study delay-induced resonances in the classical ENSO problem. This is an ideal showcase problem for bifurcation analysis because the ocean-atmosphere system of the Pacific has an oscillatory instability at the linear level due to reasonably well identified feedback effects. The resulting oscillator interacts with the annual forcing to produce a rich set of resonances [5, 6, 7] in a wide region of parameters. Extensive research has created a hierarchy of models that isolate the processes affecting ENSO; see also [8]. We explore here one of the simplest of these models that still contains physically meaningful parameters, namely, the model introduced by Tziperman *et al* [9]. This model takes the form of a scalar DDE that lumps all coupled processes into two feedback terms, which act only after given delays due to the time it takes for thermocline anomalies (proportional to sea-surface temperature anomalies) to travel across the Pacific. We provide a brief summary of the motivation behind this delayed-feedback oscillator model of ENSO in Section 2; for an account of the modelling of the processes involved at coarse to intermediate levels of complexity see the review [8] and the textbook [4].

Once a DDE model, such as that for ENSO, has been derived, the task is to understand its behaviour in dependence on relevant parameters. A quite straightforward method for investigating the eventual or attracting behaviour of a given mathematical model is its simulation by numerical integration. However, when one wants to find all possible behaviour by simulation, one is faced with a number of challenges. One generally needs to perform many simulation runs for different parameter values, for example, chosen from some sufficiently fine grid; each such run needs to be performed until transients die out sufficiently and care needs to be taken in the choice of the initial condition, especially in the presence of multistability. Note that for DDEs one needs an entire history segment as initial condition [10], making the search space infinite dimensional. Furthermore, there is the difficulty of representing and identifying, ideally automatically, what the eventual dynamics actually is.

An alternative to simulation is *bifurcation analysis*. It was orginally developed as a mathematical tool to classify the long-term behaviour of nonlinear dynamical systems that are modelled by low-dimensional ordinary differential equations (ODEs) or maps. The underlying idea is that one studies equilibria and periodic orbits and their stability and other properties as a function of relevant system parameters. When a parameter is varied, one may observe well-defined qualitative changes of the dynamics, which are referred to as bifurcations. The goal of bifurcation analysis is to find the *bifurcation diagram*, which divides the parameter space into regions of qualitatively different behaviour. A bifurcation diagram is effectively a 'road map' of where in parameter space one may find which kind of behaviour, and what changes occur in the transition from one type of behaviour to another. In spite of their seeming simplicity, ODE models of quite low dimension (such as the well-known Lorenz and Rössler systems) can already give rise to intricate bifurcation diagrams with regions of stationary, periodic, quasiperiodic and even chaotic behaviour; see, for example, the textbooks [11, 12, 13] as entry points to bifurcation theory.

Today, the bifurcation analysis of a given ODE can be performed routinely with freely available numerical tools, such as the packages AUTO [14] and MatCont [15]; see also the survey [16]. These tools only require knowledge of the right-hand side of the ODE and allow the user to perform a systematic exploration of the bifurcation diagram. This is achieved by finding and then tracking (or continuing) equilibria, periodic orbits, and their bifurcations to yield stability boundaries of the different types of solutions. The usefulness of bifurcation

theory has been demonstrated in numerous studies of ODE models arising in diverse fields of science; see, for example, [17].

More recently, numercial bifurcation tools have been implemented also for more general classes of systems. For complex models, which are typically based on partial differential equation formulations, numerical routines are available as libraries [18]. Review [19] discusses bifurcation analysis techniques specifically for fluid dynamics problems (which are the dynamical core of climate models). Textbook [4] gives an introduction to bifurcation analysis in oceanography and demonstrates the role it can play (it uses ENSO as one of its case studies). Specifically for DDEs, numerical methods for their bifurcation analysis are today available in the form of the packages `DDE-Biftool` [20] and `knut` [21]. These numerical tools apply to general systems of DDEs, including DDEs with several delays and periodic forcing. In the same way as for ODEs, these tools can determine and track the stability properties and bifurcations of equilibria and periodic orbits. As we will demonstrate, this means that numerical bifurcation studies can be performed efficiently today also for models that feature delays; see also the survey [22].

The most obvious application areas of bifurcation analysis are those where systems under consideration have tunable parameters that the practitioner can adjust to achieve the desired behaviour [11]; concrete such examples are engineering and laser physics. The situation in climate science, on the other hand, is very different in that tuning a parameter is typically not possible in the real system. In spite of this fact, we argue that systematic parameter studies are still relevant in this context, namely to determine the sensitivity of the model under consideration to changes of parameters that are known only in an order-of-magnitude sense. The fact that the observed behaviour of a nonlinear system may depend critically on all parameters motivates the bifurcation analysis with respect to selected difficult-to-determine parameters; see [23] for an exemplary study.

For our specific example, two parameters that affect the ENSO resonances strongly are the mean and the annual variation of the ocean-atmosphere coupling. The values of these two parameters are hard to ascertain in the real system; furthermore, they are also difficult to compare and convert between models of different complexity. Hence, it makes perfect sense to locate a chosen resonance tongue in the given model to restrict the values of these two parameters. When one attempts to locate a particular resonance one encounters the problem that the only places where one knows the frequency ratio analytically (or at least numerically without a scan of the complete parameter plane) are the small-forcing and the small-oscillation-amplitude regimes. In these two regimes resonance tongues are extremely narrow, and convergence to the resonant orbits (if they are stable) is very slow. This makes resonances hard to observe and track with simulations in the small-amplitude regime (corresponding to the classical devil's staircase scenario [5]). In this paper we show how this difficulty can be overcome with numerical bifurcation analysis. More specifically, periodic orbits are tracked as solutions of a boundary-value problem (BVP) and, as such, these computations are unaffected by the instability (or weak stability) of the periodic orbit under consideration or by its sensitive dependence on parameters. With this BVP approach we have tracked the relevant resonance tongues directly from their root point near the linear regime over a considerable region of the parameter plane. This bifurcation diagram, shown in Figure 6 of Section 4 below, constitutes our main result which demonstrates the capabilities of numerical bifurcation analysis in the context of climate science.

parameter	value (units)	interpretation
τ_1	1.15 (months)	time it takes warm equatorial SST perturbations from central Pacific to reach eastern boundary (via Kelvin wave),
τ_2	5.75 (months)	time it takes cold off-equatorial SST perturbations from central Pacific to reach eastern boundary (first westward via Rossby wave, then eastward via reflected Kelvin wave),
b	1/120 (per day, 0.2535 per month)	amplification factor of warm perturbations,
c	1/160 (per day, 0.1901 per month)	attenuation factor of cold perturbations,
d	1/190 (per day, 0.1601 per month)	attenuation due to dissipation,
$G(\kappa h)$	defined in Eq. (2.2)	ocean-atmosphere coupling (saturation nonlinearity),
$\kappa(t)$	$\kappa(t) = k_0 + d_k \sin(\omega t)$	annually varying slope of G at $h = 0$,
ω	$2\pi/12$ (per month)	frequency of annual variation (period $T = 12$ months),
$b_\pm$	$b_+ = 3,\ b_- = -1$	maximum and minimum of saturation nonlinearity in G.

Table 1: Values and interpretation of parameters in (2.1)–(2.3)

2. ENSO as a parametrically forced delayed-feedback oscillator

We consider a conceptual model for the ENSO mechanism that simplifies the circulation of ocean surface water waves and the ocean-atmosphere interaction to a scalar DDE, which is periodically forced due to the annual variation of the strength of ocean-atmosphere coupling. We use the parameters and follow the notation of [9], where the dependent variable is the height anomaly $h(t)$ of the thermocline at the Eastern boundary of the Pacific. The height anomaly h (in dimensionless units) satisfies

$$\frac{\mathrm{d}}{\mathrm{d}t}h(t) = bG\left[\kappa(t - \tau_1)h(t - \tau_1)\right] - cG\left[\kappa(t - \tau_2)h(t - \tau_2)\right] - dh(t), \text{ where} \tag{2.1}$$

$$G(x) = \begin{cases} b_+ \tanh(x/b_+) & \text{if } x \geq 0, \\ b_- \tanh(x/b_-) & \text{if } x < 0, \end{cases} \tag{2.2}$$

$$\kappa(t) = k_0 + d_k \sin(\omega t). \tag{2.3}$$

The right-hand side of (2.1) combines positive feedback due to the warm equatorial sea-surface temperature (SST) perturbation in the central Pacific, negative feedback due to the cold off-equatorial SST perturbation in the central Pacific, and dissipation. The parameters and their values used here are from Tziperman *et al* [9], and they are listed in Table 1.

The idea that a dynamical instability is the basic mechanism behind ENSO was first proposed by Bjerknes in 1969 [24]. The review by Neelin *et al* [8] describes the hierarchy of models that have been developed during the following decades. The textbook [4] presents a detailed walk-through of this hierarchy, including a derivation of delayed-feedback oscillator models very similar to (2.1). The more complex models in this hierarchy help to establish which physical processes are connected. The simpler models, such as (2.1) considered here, take these connections for granted and treat them as lumped positive or negative feedback terms in the right-hand side. Figure 1 sketches the physical processes that enter the right-hand side of (2.1) and their connections. The height of the thermocline is a proxy for
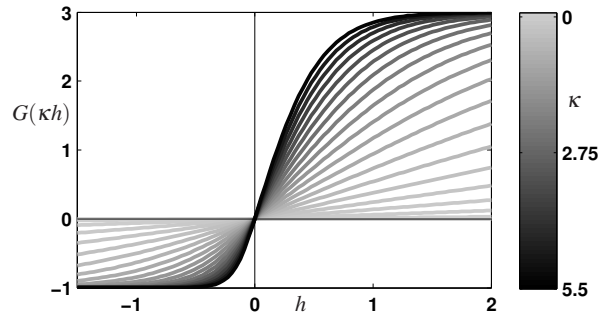
Figure 1: Schematic of the two feedback mechanisms that motivate the ENSO model (2.1). The shading of the ocean corresponds to the thermocline (and sea-surface temperature) in equilibrium: darker means lower (colder). Equation (2.1) only describes the anomaly of the thermocline, h, at the eastern boundary. The labels h_{ec} and h_{oc} refer to the thermocline anomaly in the equatorial and the off-equatorial central pacific, respectively, which feed into the feedback mechanisms. Regular arrows indicate same-sign re-inforcement and horizontal (inhibition) bars indicate oppposite-sign re-inforcement; the label on each arrow shows the time delay of the interaction.

the sea-surface temperature. In equilibrium the thermocline is low at the eastern boundary of the Pacific and high at the western end. This difference maintains an atmospheric convective loop above the equatorial ocean, which points westward at the ocean surface because the relatively cold water at the eastern end cools the atmosphere, causing air to sink (and vice-versa, the relatively warm water at the western end heats up the atmosphere, causing air to rise). The dependent variable h in (2.1) measures the anomaly of the thermocline at the eastern boundary, that is, the deviation from equilibrium at this point.

A disturbance in the atmospheric convective loop, that is, a slowing down of the westward surface wind (creating an eastward wind stress of the ocean surface) in the central Pacific causes surface water transport toward the equator. Surface water is warm, causing an increase of h in the equatorial central Pacific, and a decrease of h in the off-equatorial central Pacific. The positive thermocline disturbance at the equator travels eastward along the equator (in a *Kelvin wave*), and hits the eastern boundary after time τ_1. The corresponding increase in sea-surface temperature at the eastern boundary slows down the atmospheric convection (the relatively cold water at the eastern boundary is a driver of the convection). This creates the first, positive feedback term in (2.1) with the delay τ_1 (note that $b > 0$).

The off-equatorial depression of h travels westward and toward the equator (in a *Rossby wave*), reflects at the western Pacific boundary, and then travels as a Kelvin wave eastward, reaching the eastern boundary after time τ_2. The depression of h corresponds to a cooling down of the sea surface such that atmospheric convection is enhanced, creating the negative delayed feedback term in (2.1) with the delay τ_2 (note that $c > 0$).

The above effects work all at the linear level of the disturbance of the equilibrium. The nonlinearity in (2.1) comes from saturation and asymmetry in the ocean-atmosphere coupling instability, as expressed by the function G in (2.2) that is shown in Figure 2. Moreover, the slope of G at $h = 0$ varies throughout the year, being strongest in the northern summer and weakest in the winter; see [9] for a realistic time profile of the annual variation. This annual variation is expressed in the sinusoidal variation (2.3) of the pre-factor κ in the argument of G. Since only the amplification factor varies in time, the oscillator described by (2.1) is *parametrically excited*; in particular, the equilibrium $h = 0$ of the unforced system

Figure 2: Profile of coupling function $G(\kappa h)$ for $\kappa \in 0,\ldots,5.5$, which are the values that are encountered in the parameter range $(d_k, k_0) \in [0, 2.5] \times [0, 3]$.

(for $d_k = 0$) corresponds to a trivial periodic solution in the periodically-forced system (for $d_k > 0$).

3. Delay differential equations and their bifurcations analysis

This section is a short review of the general theory of dynamical systems with delays as needed for the bifurcation analysis of the ENSO model in Section 4, which the reader may wish to consult already for illustrations of the concepts introduced now. To keep the exposition specific to the ENSO model under consideration, we present the theory for the case that the right-hand side of the DDE depends on the current value of the dependent variable, as well as on two values from the past, with delays $\tau_1 \le \tau_2$. Furthermore, we allow the right-hand-side of the DDE to depend explicitly on time, which accounts for the periodic forcing of (2.1). Hence, we consider a DDE of the form

$$\frac{\mathrm{d}}{\mathrm{d}t}x(t) = f(t, x(t), x(t - \tau_1), x(t - \tau_2), \eta), \tag{3.1}$$

where $x \in \mathbb{R}^n$ is an n-dimensional state and $\eta \in \mathbb{R}^m$ is a multi-parameter; one also refers to $\mathbb{R}^n$ as the physical space. The function

$$f : \mathbb{R} \times \mathbb{R}^n \times \mathbb{R}^n \times \mathbb{R}^n \times \mathbb{R}^m \to \mathbb{R}^n$$

describes the right-hand-side, and it is assumed to be sufficiently smooth. Note that (3.1) is non-autonomous because f depends explicitly on time t. We consider here only the case of periodic forcing, that is, $f(t, \cdot, \cdot, \cdot, \eta) = f(t + T_f, \cdot, \cdot, \cdot, \eta)$ where T_f is the forcing period. An important special case is that the forcing amplitude is zero, so that system (3.1) is autonomous. We assume here that the forcing amplitude is one of the components of the parameter vector η, so that the limiting autonomous case can be found as a subset of parameter space.

We proceed to discuss the basic properties of the DDE (3.1), both for the autonomous and the non-autonomous cases, which form the basis of the bifurcation analysis of the ENSO model in Section 4. We remark that the theory presented here is also valid for more general DDEs, including those with distributed delays, as long as all delays are constant and bounded. Full technical proofs can be found in the classical textbooks by Hale and Verduyn-Lunel [10] and Diekmann *et al* [25]; the textbook by Stépán [2] is also rigorous, but provides a shorter route to those parts of the theory that are necessary for practical applications.

Because of the presence of delayed terms, the DDE (3.1) does not define a dynamical system on the physical space $\mathbb{R}^n$. Rather, its phase space is the infinite-dimensional space $\mathbb{R} \times C([-\tau_2, 0]; \mathbb{R}^n)$; here $\mathbb{R}$ represents time and $C([-\tau_2, 0]; \mathbb{R}^n)$ is the space of continuous functions over the maximal delay interval $[-\tau_{\max}, 0] = [-\tau_2, 0]$ with values in the physical space $\mathbb{R}^n$. This means that in order for the initial-value problem to be well defined one needs to prescribe an entire function $x_0 : [-\tau_2, 0] \to \mathbb{R}^n$ as the initial condition. Similarly, after solving (3.1) from time 0 to time t the current state is the function $x_t : [-\tau_2, 0] \to \mathbb{R}^n$ given by $x_t(s) = x(t+s)$, $s \in [-\tau_2, 0]$. These trajectories x_t in the infinite-dimensional phase space $\mathbb{R} \times C([-\tau_2, 0]; \mathbb{R}^n)$ depend smoothly on the initial condition x_0, meaning that classical dynamical systems theory can be applied to the DDE (3.1) in $\mathbb{R} \times C([-\tau_2, 0]; \mathbb{R}^n)$. When the forcing amplitude is zero the time axis decouples and it is sufficient to study the autonomous DDE with phase space $C([-\tau_2, 0]; \mathbb{R}^n)$.

(a) *Equilibria and their bifurcations*

We first consider the case that f is autonomous, which is of interest on its own as well as in the context of periodic forcing where it corresponds to zero forcing amplitude. An equilibrium or steady state is an initial function $x_0 : [-\tau_2, 0] \to \mathbb{R}^n$ in phase space such that $x_t(s) = x_0(s)$ for all $s \in [-\tau_2, 0]$ and $t > 0$. Hence, $x_0(s)$ equals a constant $\bar{x}_0$ for all $s \in [-\tau_2, 0]$ and the constant vector $\bar{x}_0 \in \mathbb{R}^n$ can be determined from the equation

$$f(\bar{x}_0, \bar{x}_0, \bar{x}_0, \eta) = 0, \tag{3.2}$$

which, as for ODEs, is a system of n algebraic equations. This means that equilibria of DDEs can be found and tracked in a parameter as roots of (3.2) by standard continuation methods.

To determine the stability of an equilibrium x_0 one moves it to the origin and linearises the DDE. The result is a linear DDE of the form

$$\dot{x}(t) = Ax(t) + Bx(t - \tau_1) + Cx(t - \tau_2),$$

where A, B and C are $n \times n$ matrices. The stability of the origin is determined by the spectrum of the eigenvalues of the linearisation, which can be found as the roots of the *characteristic function*

$$\chi(\lambda) = \det(\lambda I - A - Be^{-\lambda \tau_1} - Ce^{-\lambda \tau_2}), \tag{3.3}$$

where I is the $n \times n$ identity matrix. The characteristic function χ of a linear autonomous DDE (of the type considerd here) has at most finitely many roots with non-negative real part [10, 2]. This means that the stability theory of equilibria of DDEs is very similar to that for ODEs. An equilibrium is stable if all eigenvalues of its linearisation have negative real part. It changes its stability type when eigenvalues cross the imaginary axis of the complex plane. When a single parameter is varied there are two typical scenarios, which give rise to the standard local bifurcations of equilibria of codimension one [11, 12, 13]:

- when a single real eigenvalue goes through zero the bifurcation then one encounters, in the generic case, a *saddle-node bifurcation*, where two equilibria meet and dissaper (or are created); in the presence of additional properties of the equation (such as symmetries) one encounters a *branch bifurcation*, where two additional equilibria bifurcate;

- when a complex conjugate pair of eigenvalues moves across the imaginary axis of the complex plane then one encounters a *Hopf bifurcation* from which a small periodic orbit bifurcates.

These bifurcations of autonomous DDEs can be detected and tracked as for ODEs by fixing the real parts of roots of the characteristic function χ in (3.3) to zero and freeing a second parameter (such that $\eta \in \mathbb{R}^2$). In this way, one can compute curves of saddle-node/branch and Hopf bifurcations in a two-dimensional parameter space. The curves divide the parameter plane into regions where different numbers and types of equilibria exist.

(b) *Periodic orbits and their bifurcations*

An initial function x_0 is a periodic point of the DDE (3.1) if it satisfies $x_{T_\Gamma}(s) = x_0(s)$ for all $s \in [-\tau_2, 0]$ and some $T_\Gamma \geq 0$, where T_Γ is called the (minimal) period of x_0. Practically, one finds a periodic point of (3.1) as a *periodic orbit*, which is a closed curve $\Gamma : [0,1] \mapsto \mathbb{R}^n$ in the physical space satisfying the *periodic boundary-value problem*

$$\dot{\Gamma}(t) = T_\Gamma f(t, \Gamma(t), \Gamma(t - \tau_1/T_\Gamma)_{\mathrm{mod}[0,1]}, \Gamma(t - \tau_2/T_\Gamma)_{\mathrm{mod}[0,1]}, \eta) \quad \text{for } t \in (0,1],$$
$$\Gamma(0) = \Gamma(1). \tag{3.4}$$

The notation $\Gamma(t - \tau_j/T_\Gamma)_{\mathrm{mod}[0,1]}$ means that for combinations of t, τ_j and T_Γ for which $t - \tau_j/T_\Gamma$ is outside of the interval $[0,1]$ we choose the appropriate integer ν such that $t - \tau_j/T_\Gamma + \nu \in [0,1]$ and evaluate $\Gamma(t - \tau_j/T_\Gamma + \nu)$. From any solution Γ of (3.4) one can find periodic points x_0 of period T_Γ through the relationship

$$q(s) = \Gamma(s/T_\Gamma)_{\mathrm{mod}[0,1]} \quad \text{for } s \in [-\tau_2, 0]. \tag{3.5}$$

When the DDE is autonomous then the period T_Γ in (3.4) is one of the unknowns that must be found together with Γ. This can be done in the same way as for ODEs by the adding one scalar equation, a so-called *phase condition* [26], which determines T_Γ and makes the solution Γ of (3.4) locally unique. Good starting points for periodic orbits of autonomous DDEs are Hopf bifurcations where small-amplitude periodic orbits branch off. Their period T_Γ is determined by the imaginary part of the pair of purely complex conjugate eigenvalues at the Hopf bifurcation.

   The situation is different when the DDE is periodically forced. Then there are no equilibria, and the simplest invariant object is a periodic orbit Γ whose period equals the forcing period T_f, that is, $T_\Gamma = T_f$ is known in (3.4). In fact, each equilibrium $x_0(s) = \bar{x}_0$, $s \in [-\tau_2, 0]$ of the autonomous system for zero forcing amplitude gives rise to a trivial periodic orbit of the form $\Gamma_0(t) \equiv \bar{x}_0$. The trivial periodic orbit Γ_0 can then be continued as a periodic orbit Γ of the periodically-forced DDE when the forcing is increased from 0. For the special case that the forcing is parametric, as in the ENSO model (2.1), one finds that $\Gamma(t) = \Gamma_0(t) \equiv 0$ remains constant for all forcing amplitudes; however, in general, $\Gamma(t)$ is a non-constant periodic function when the forcing is nonzero; note that generically the period of any periodic orbit of a periodically-forced DDE is an integer multiple of the forcing period. Periodic orbits can generally not be found analytically, but the boundary value problem (3.4) can be solved numerically with the same numerical methods (for example, with Gauss collocation) that are used to compute periodic orbits of ODEs [22].

   The stability of a periodic orbit Γ is determined by its Floquet multipliers μ_i, which are the eigenvalues of the time-T_Γ map of the point x_0 on the periodic orbit Γ given by

(3.5). If all μ_i are inside the unit circle of the complex plane then Γ is stable; conversely, the eigendirections of the Floquet multipliers outside the unit circle correspond to unstable directions. Similarly to the case of equilibria, for a time-periodic DDE one can construct a characteristic function $\chi_p(\mu)$ such that the Floquet multipliers of Γ are the roots of χ_p [21, 27]. Generally, the characteristic function χ_p and its roots are found numerically, after one has computed Γ and its period T_Γ [28]. For a DDE there are infinitely many roots of χ_p and, hence, Floquet multipliers μ_i, but they are also discrete and have the origin of the complex plane as their only accumulation point; in particular, there are at most finitely many unstable Floquet multipliers. As for ODEs, a periodic orbit changes its stability when Floquet multipliers cross the unit circle, and this gives rise to the same well-known local bifurcations of periodic orbits. When a single parameter is varied there are three typical scenarios, which give rise to the standard generic local bifurcations of periodic orbits of codimension-one [11, 12, 13]:

- when a single real Floquet multiplier goes through $+1$ then one encounters a *saddle-node bifurcation of limit cycles*, where two periodic orbits meet and disappear (or are created);

- when a single real Floquet multiplier goes through -1 then one encounters a *period-doubling bifurcation*, where a periodic orbit of twice the period bifurcates;

- when a complex conjugate pair of eigenvalues goes through the unit circle at $e^{\pm 2\pi\alpha i}$ then one encounters a *Neimark-Sacker or torus bifurcation*, where a smooth invariant torus bifurcates (provided that low-order resonances are avoided, that is, $\alpha \neq 1, 1/2, 1/3, 2/3, 1/4, 3/4$).

An example where bifurcations of the trivial periodic orbit can be found analytically is the delayed Mathieu equation (also a parametrically forced system) [29]. More generally, however, these bifurcations of DDEs need to be detected and tracked numerically as for ODEs, by appending the above conditions on the Floquet multipliers to the continuation of the periodic orbit. In this way, one can compute curves of saddle-node of limit cycle, period-doubling and torus bifurcations of DDEs in a two-dimensional parameter space.

(c) *Resonances and quasiperiodicity*

Resonant periodic orbits are special periodic orbits that correspond to the locking of two different oscillations of the system. They are organised in DDEs in *resonance tongues* and *resonance surfaces* in the same way as in ODEs; see Figure 6 later and, for example, [30, 31] for the general theory for ODEs. Along a torus bifurcation curve in a parameter plane a Floquet multiplier $e^{\pm 2\pi\alpha i}$ moves along the unit circle, that is, the quantity α changes. When $\alpha = k/\ell \in \mathbb{Q}$, a two-parameter family of $k : \ell$ resonant periodic orbits (a so-called resonance surface) branches off. The projection of this surface onto the parameter plane is a resonance tongue, which is a region in the parameter plane where periodic orbits exist that are $k : \ell$ locked to the original periodic orbit (or to the forcing period in a forced DDE, such as the parametrically forced ENSO model). Inside the resonance tongue there are initially two periodic orbits, one of which is always unstable. The root point of the resonance tongue is attached to the bifurcation curve. Close to the root point the two periodic orbits form $k : \ell$ torus knots. In a cross section transverse to the flow one finds a period-ℓ orbit; the return map to the cross section acts on it by mapping each point to its kth neighbour in the counter-clockwise direction. If the denominator ℓ is also greater than 4 both periodic orbits

lie on an invariant torus (close to the root point this is guaranteed by general theory [13]), one periodic orbit is stable within the torus, one is unstable.

Similarly, one finds resonance tongues that are rooted at a line in the parameter plane where the forcing is zero. At such a root point of the $k : \ell$ resonance tongue the unforced system has a periodic orbit Γ such that the ratio of its period T_Γ and the forcing frequency T_f is $\alpha = k/\ell \in \mathbb{Q}$.

By contrast, when α is irrational, that is, $\alpha \notin \mathbb{Q}$, then there is a smooth curve in the parameter plane starting at the corresponding point on the torus bifurcation curve, or line of zero forcing, along which one finds a torus that is densely filled by a quasiperiodic trajectory. The overall scenario is one of a complicated interplay between locked and quasiperiodic dynamics on the bifurcating torus. In particular, if one plots the rotation number along any parameter path that intersects the resonance tongues one finds the well-known devil's staircase consisting of infinitely many intervals where the rotation number is constant (inside the resonance tongues), as also observed in simulations of ENSO models [5, 6, 7].

A resonance tongue is bounded near its root point by saddle-node of limit cycle bifurcation curves of the two orbits existing inside. An alternative method to the simulations as done in [5, 6, 7] is to compute the $k : \ell$ resonance surface by using the periodic BVP (3.4) with period $T_\Gamma = \ell T_f$ and two free parameters. In this way one obtains a surface consisting of all locked periodic orbits inside the resonance tongue. This compuation can be started at any point with rational α on the torus bifurcation curve or the line where the system is unforced. The continuation of the locked periodic orbits is numerically robust, and the resonance tongue is obtained by projection onto the parameter plane. This method has been introduced in [31, 32] for the computation of resonance surfaces in maps and forced ODEs; Appendix A explains how it can be adapted and implemented for a general DDE of the form (3.1).

(d) Ready-to-use software for the bifurcation analysis of DDEs

`DDE-Biftool` is a collection of `Matlab` functions that perform each necessary task and that can be called by the user. For example, there exist functions for calculating the eigenvalues of a given equilibrium, the Floquet multipliers of a periodic orbit, for converting a periodic BVP into a large (discretised) nonlinear system, for solving nonlinear equations with Newton iteration, for adapting the mesh on a given periodic solution, and for tracking solutions of nonlinear systems if one has one more free parameter than equations. Curve tracking of equilibria in a single parameter, of codimension-one bifurcations of equilibria in two parameters, and of periodic orbits of autonomous DDEs in a single parameter have been implemented. Codimension-one bifurcations of periodic orbits can be detected, but tracking them requires one to define a suitable extended system manually. Because `DDE-Biftool` permits one to add an arbitrary number of conditions and parameters to the system, it is possible to track solution surfaces instead of curves. We make use of this feature for the computation of resonance tongues; see Appendix A.

The package `knut` (formerly known as `PDDE-Cont`) is a stand-alone alternative to `DDE-Biftool`. Its numerical methods are summarised in the review article by Roose and Szalai [22] and in [21].
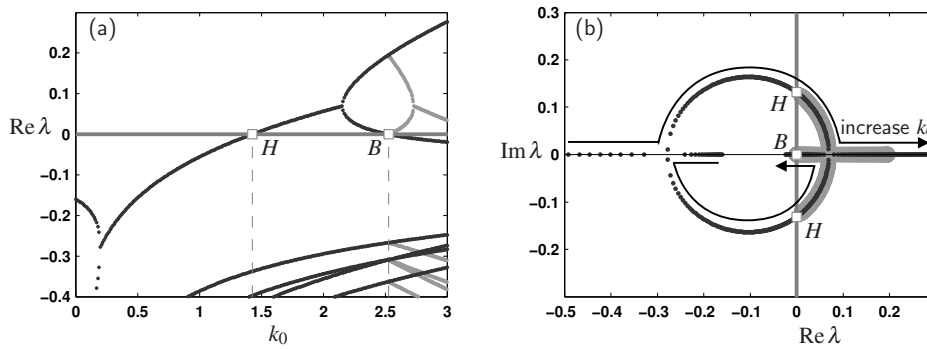
Figure 3: Stability of the trivial equilibrium $h \equiv 0$ and of bifurcating secondary equilibria of (2.1) for $d_k = 0$ as a function of k_0. Panel (a) shows the real parts of the eigenvalues of the equilibria as a function of k_0, and panel (b) shows the locus of the two leading eigenvalues in the complex plane; the eigenvalues of $h \equiv 0$ are plotted in black and those of the bifurcating equilibria in grey.

4. Bifurcation analysis of the ENSO model

The main conclusion of Tziperman *et al* [9] was that in model (2.1) the peak of the ENSO is locked to the end of the year, which corresponds to the minimum of the excitation $\kappa(t)$. That is, if $\kappa(t) = k_0 + d_k \sin(t\pi/6)$ such that the period of κ is 12 (time is in unit of months), then the maximum of the thermocline anomaly, h, occurs at $t \approx 8 \ldots 9 + 12\ell$ where ℓ is the denominator of the resonance. In [9] the parameters were chosen such that $\ell = 3$, so the ENSO peak occured every three years. The authors also stated that in all their simulations they found the locking to the peak to the end of the year to be extremely robust with respect to all parameters.

    We demonstrate here how the phenomenon of delay-induced resonances can be studied systematically by means of a bifurcation analysis of (2.1). More specifically, we determine all $k : \ell$ resonance tongues with $\ell \leq 11$ in the relevant region of the (d_k, k_0)-plane of mean k_0 versus annual variation d_k of the amplification factor in (2.3); they are chosen as the bifurcation parameters since the interaction between ocean and atmosphere is known only qualitatively as expressed by the function G shown in Figure 2. In contrast, confidence in the other parameters of (2.1) is higher: the delays τ_1 and τ_2 are known with good accuracy, and the relation between damping and feedback effects can be estimated directly from observations (involving only oceanic quantities). These other parameters are fixed at the values from [9]; see Table 1.

(a) The autonomous regime for $d_k = 0$

The starting point of our bifurcation analysis is the autonomous case where $d_k = 0$. Then $h \equiv 0$ is an equilibrium irrespective of the value of k_0, and we know that it is stable for $k_0 = 0$. We proceed to continue this equilibrium with the package `DDE-Biftool` [20] over the range $k_0 \in [0, 3]$ while monitoring its stability. The behaviour of the eigenvalues of $h \equiv 0$ is illustrated by the black curves in Figure 3. Panel (a) shows how the real part of the eigenvalues changes with k_0, and panel (b) how the two leading eigenvalues move in the complex plane with increasing k_0. The trivial equilibrium $h \equiv 0$ is initially stable and then loses its stability at $k_0 \approx 1.426$ in a Hopf bifurcation H, where a complex pair of eigenvalues crosses the imaginary axis. At $k_0 \approx 2.158$ the complex pair meets on the real line
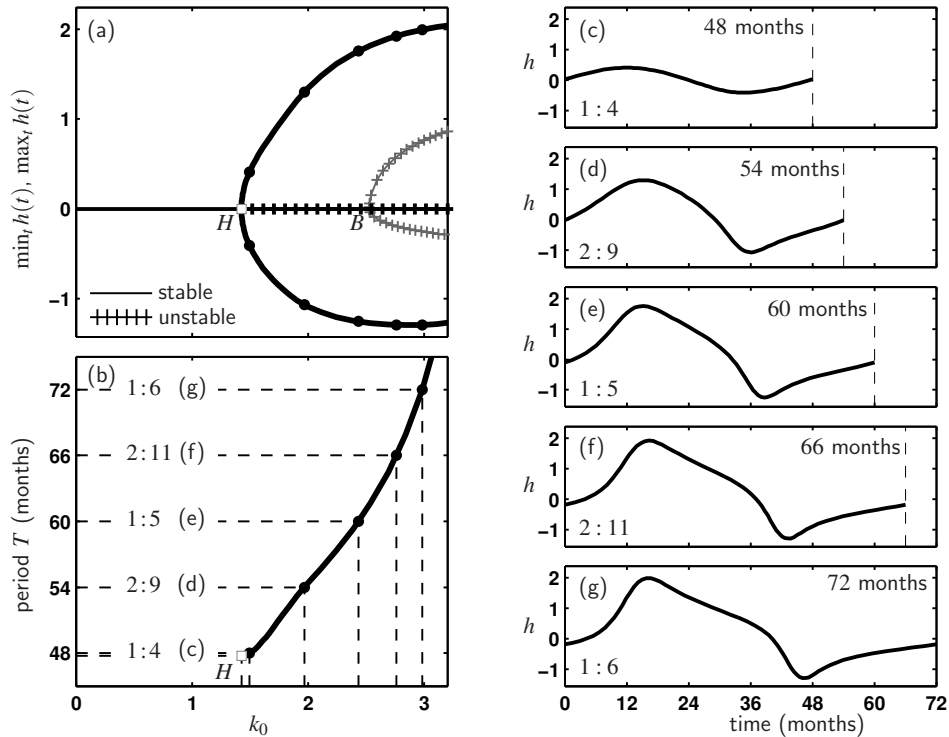
Figure 4: Single-parameter bifurcation diagram (a) of the autonomous system (2.1) for $d_k = 0$ and varying k_0. The equilibrium $h \equiv 0$ loses stability at the Hopf bifurcation H; a branch of secondary equilibria emerges from the branch point B. Panel (b) shows the period T along the branch of stable periodic orbits that bifurcates from H, and panels (c)–(g) show time profiles of the indicated low-order resonant periodic orbits along the branch.

of the complex plane and splits up into two real eigenvalues. One of these real eigenvalues decreases and crosses the origin of the complex plane at $k_0 \approx 2.526$ (the point is labelled B in Figures 3 and 4). Physically, at B the positive feedback terms in (2.1) exactly cancel the damping and the negative feedback for $h = 0$, and a branch of two nonzero equilibria bifurcates and exists for k_0 past B. We continued these equilibria, and their eigenvalues are shown as grey curves in Figure 3. There is a pair of positive real eigenvalues and, hence, the secondary equilibria are unstable in the range $k_0 \in [2.526, 3]$.

Figure 4(a) shows the one-parameter bifurcation diagram for $k_0 \in [0, 3]$. The equilibrium $h \equiv 0$ loses its stability at H, and at the branch point B the branch of secondary, unstable equilibria emerges. Also shown in Figure 3(a) is the branch of bifurcating periodic orbits as computed by continuation with DDE-Biftool from the Hopf bifurcation point H. The periodic orbits are represented by plotting their minina and maxima; they are all stable, as was checked with the computation of the Floquet multipliers (not shown). Of special interest are those periodic orbits along the branch that give rise to low-order resonances with the forcing period of $T_f = 12$ months (once the annual variation of the amplification is turned on, that is, d_k is increased from 0). Figure 4(b) shows the period T_Γ of the periodic orbits along the branch, where all $k : \ell$ resonant periodic orbits with $\ell \leq 11$ are indicated — from the 1 : 4 resonance very close to the Hopf bifurcation H to the 1 : 6 resonance at $k_0 \approx 2.982$. Panels (c)–(g) show the respective time profiles of these resonant periodic orbits.

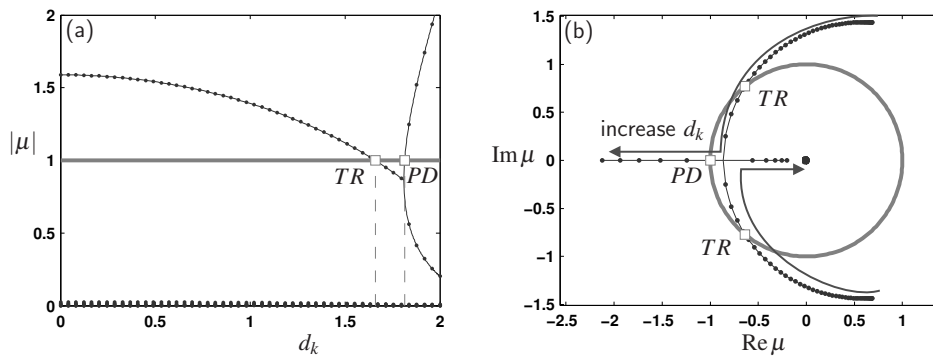Figure 4 gives a complete picture of the autonomous dynamics of (2.1) for $d_k = 0$. Notice

Figure 5: Stability of the trivial periodic solution $h \equiv 0$ as a function of the forcing d_k for $k_0 = 1.8$. Panel (a) shows the Floquet multipliers as a function of d_k, and panel (b) shows the locus of the two leading Floquet multipliers in the complex plane.

further from Figure 3(a) that all but the two leading eigenvalues have quite large negative real parts. This suggests that the dynamics of the DDE (2.1) behaves like a two-dimensional ODE with parametric periodic forcing for $k_0 \leq 3$ and delays that are realistic for the ocean. For this reason, the bifurcation diagram of the autonomous DDE is fairly simple. This is in contrast to the much more complex bifurcation diagrams when the delays become large enough to shift a large number of eigenvalues close to the imaginary axis [33].

(b) *The dynamics with periodic forcing for $d_k > 0$*

We now perform a bifurcation analysis of the periodically-forced DDE (2.1) for $d_k > 0$. The trivial periodic solution $h \equiv 0$ for $d_k = 0$ gives rise for $d_k > 0$ to a periodic orbit with period T_f. Owing to the parametric nature of the periodic forcing, this periodic orbit has zero amplitude, that is, it remains the trivial solution $h \equiv 0$. As was the case for the equilibria in the autonomous case, the main question is when $h \equiv 0$ is stable. This can be determined by its continuation in d_k for fixed k_0. Figure 5 shows how the Floquet multipliers of the trivial periodic orbit $h \equiv 0$ change as d_k is increased for fixed $k_0 = 1.8$, which is the value that was used in [9]. For $(k_0, d_k) = (1.8, 0)$ the periodic orbit $h \equiv 0$ is initially unstable, since a single pair of complex conjugate Floquet multipliers lies outside the unit circle. At $d_k \approx 1.659$ this complex conjugate pair crosses the unit circle and $h \equiv 0$ undergoes a torus bifurcation, labelled TR, and becomes stable. When d_k is increased further, the complex conjugate pair comes together on the real line of the complex plane at $d_k \approx 1.810$ and then splits up into two real Floquet multipliers. Very soon thereafter, at $d_k \approx 1.814$, one of them decreases and crosses the unit circle at -1 and, hence, $h \equiv 0$ undergoes a period-doubling bifurcation, labelled PD, and becomes unstable again.

   We now consider the bifurcation diagram of (2.1) in the (d_k, k_0)-plane, which is shown in Figure 6. The torus bifurcation and the period-doubling bifurcation have been continued as curves. The torus bifurcation curve TR starts at the Hopf bifurcation point on the automonous-limit line $d_k = 0$ and it ends on the period-doubling bifurcation curve PD in a 1 : 2 resonance. Below the curve TR and to the left of the curve PD the trivial periodic orbit $h \equiv 0$ is stable. To the right of the curve PD and above the curve TR the periodic orbit $h \equiv 0$ is unstable.
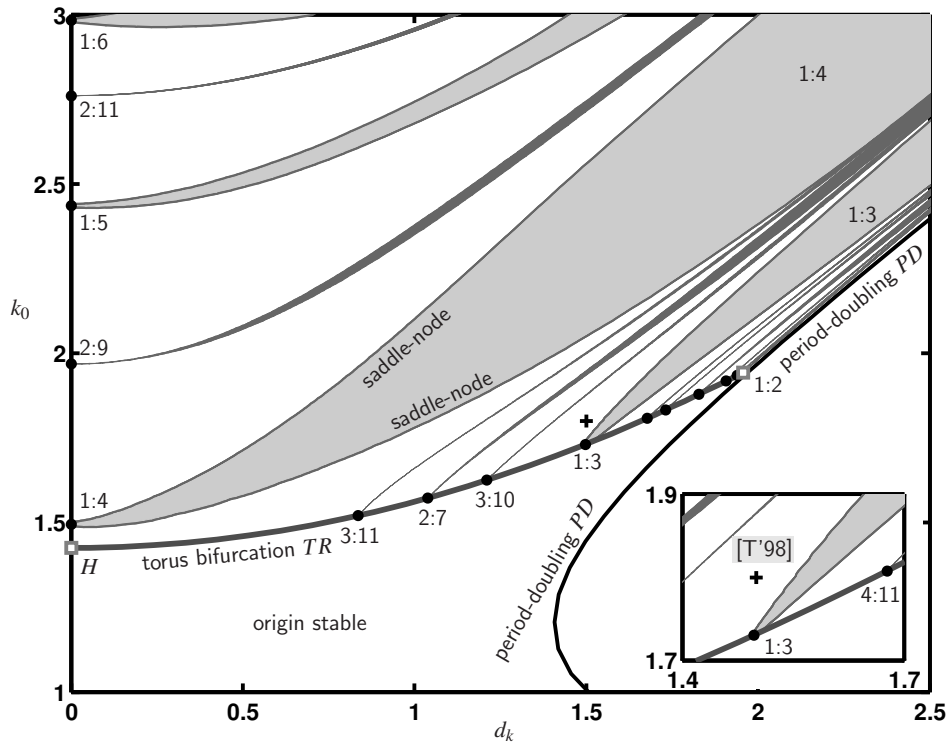
Figure 6: Two-parameter bifurcation diagram of the ENSO model (2.1) in the (d_k, k_0)-plane (d_k, k_0). All $k : \ell$ resonance tongues with $\ell \leq 11$ are shown. They are rooted at points on the autonomous boundary $d_k = 0$ and on the torus bifurcation curve TR, which ends on a period-doubling curve at a $1 : 2$ resonance. The trivial solution $h \equiv 0$ is stable in the region below the curve TR. The inset shows an enlargement near the tip of the $1 : 3$ resonance tongue; the point corresponding to the parameter values used by Tziperman *et al* [9] is marked by a cross.

(*c*) *Resonance tongues in the ENSO model*

Above the torus bifurcation curve TR one finds invariant tori and associated $k : \ell$ resonance tongues, and Figure 6 shows all resonance tongues for $\ell \leq 11$. As we have already seen in Figure 4, along the line $d_k = 0$ and above the Hopf bifurcation point H we find five root points of these resonance tongues. Additional root points of resonance tongues are found along the torus bifurcation curve TR. Specifically, we observe that the rotation number α gradually increases until the torus bifurcation curve terminates in the $1 : 2$ resonance on the period-doubling bifurcation curve PD; along TR we find nine more root points of $k : \ell$ resonance tongues with $\ell \leq 11$. The resonance tongues in Figure 6 have been computed as resonance surfaces with the method described in Appendix A; they were then projected onto the (d_k, k_0)-plane to yield the open regions of locked periodic orbits and their boundaries. Notice how, as theory states [30, 31], the resonance tongues become very narrow with increasing denominator ℓ. We found that the corresponding $k : \ell$ locked periodic orbit of the ENSO model is stable and, hence, observable practically everywhere throughout the considered parameter region (exceptions are the parts of the narrow $3 : 11$, $3 : 10$, $4 : 9$, and $5 : 11$ resonance tongues in the area where $d_k > 2$). The cross in Figure 6 shows the parameter point chosen by Tziperman *et al* [9]; it is slightly to the left of the $1 : 3$ tongue
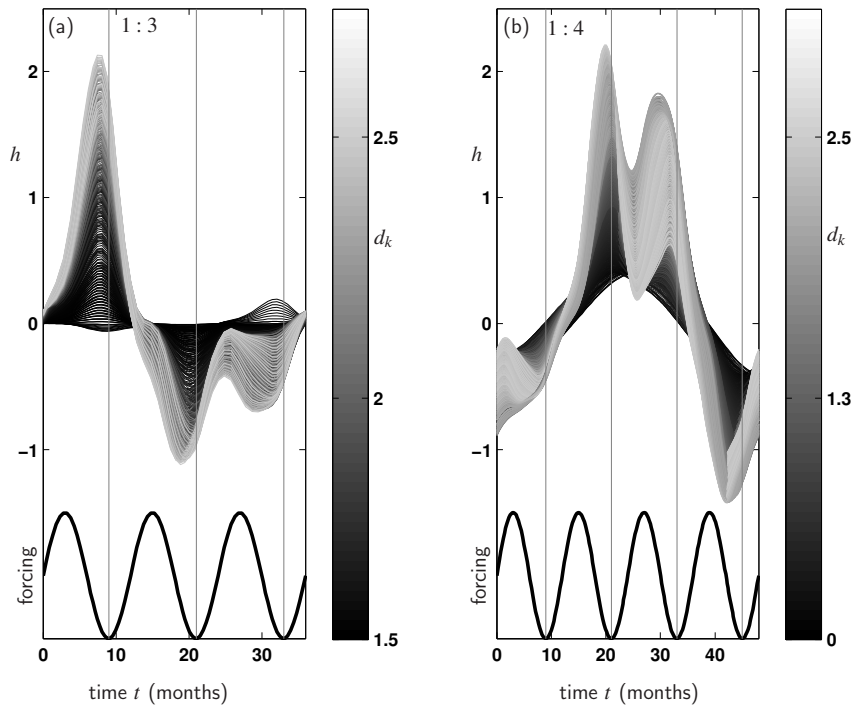
Figure 7: Locking of ENSO peak to the end of the year for all stable periodic orbits in the main tongues of $1:3$ (a) and $1:4$ resonance (b), where grayscale represents the value of d_k for which the periodic orbit is found. The black sinusoidal curve at the bottom indicates the phase of the forcing.

(see the inset), which explains that these authors observed non-periodic motion closely resembling a period-three orbit.

The other main feature observed in [9] is that the peak of the oscillations appeared to be locked to the end of the year, that is, the maximum of $h(t)$ occurs at time $t \approx 8 \ldots 9 + 12\ell$. To investigate how general this observation is Figure 7 displays the profiles of all stable periodic orbits in the main $1:3$ and $1:4$ resonance tongues, together with the forcing. We find clear evidence of phase locking to the forcing in both cases, where the stable periodic orbit reaches its maximum shortly before the forcing reaches its minimum. Since the delays τ_1 and τ_2 enter directly into the phase of the forcing of the ENSO model (2.1), it is clear that the two delays strongly influence the location of the maximum of h relative to the forcing phase. Figure 7 is evidence that the phase between h and the forcing is nearly independent of the parameters d_k and k_0. This observation provides a certain justification for a reduction of the ENSO model even further to contain only the delays and not the periodic forcing; see [34] for a demonstration of how resonances can be explored with Boolean delay equations.

5. Conclusions

We presented a bifurcation study of how delay-induced resonances organise the parameter plane of mean and variation of the annual forcing of a model of ENSO with delayed feedback and forcing. The main message is that, colloquially speaking, the bifurcation theory for the considered class of DDEs is exactly as that for ODEs, but embedded into an infinite

dimensional phase space. Hence, equilibria, periodic orbits and their bifurcations can be detected and tracked in DDEs much as for ODEs, and software packages exist for this task. As our case study demonstrates, numerical bifurcation anlysis is today perfectly feasible for periodically-forced DDEs, and it allows one to obtain insights beyond what is possible with long-time simulations.

Bifurcation analysis of equilibria and periodic orbits can give evidence for the presence of deterministic chaos via the detection of bifurcations associated with routes to chaos. A specific example is chaotic dynamics due to the break-up of tori when resonance tongues overlap. In the ENSO model the resonance tongues do not overlap in the parameter region we explored and, hence, no chaotic dynamics was found. However, when the forcing is large enough, resonance tongues will generally overlap, and the method we used of computating resonance tongues as surfaces is especially suitable in this case. Hence, bifurcation analysis can add insight into the chaotic dynamics in DDE models.

A limitation of bifurcation analysis is that chaotic behaviour can only be studied indirectly, by finding bifurcations and instabilities of equilibria and periodic orbits. In the study of climate systems this imposes restrictions on the realism of the model. For example, a realistic ocean boundary or ocean floor will introduce fluctuations even at steady-state ocean flow. Thus, bifurcation analysis in ocean and climate systems is typically performed on idealised systems [4]. These idealized systems incorporate the relevant physical effects but reduce realism such that steady states become genuine equilibria. The Zebiak-Cane model for ENSO, which provides the basis for the delayed oscillator model, is one example of such idealised systems (described in the review [8]).

Another issue in this regard is that — even for systems much simpler than climate models — it is often very hard, if not impossible, in practice to distinguish between deterministic chaos and noise-induced fluctuations in observed data. One reason for this may lie in a lack of hyperbolicity of the deterministic chaotic attractor, which makes it non-robust (that is, sensitive to arbitrarily small changes in the parameters); this non-robustness gets 'smeared out' if one adds random disturbances to the deterministic model; see [35] for a study relevant to climate dynamics. In particular, for the ENSO these two hypotheses are still competing. Whereas Tziperman *et al* [9] presented the ENSO as if it was mostly a deterministic chaotic trajectory, linear models subject to noise are also used to explain, for example, the variation in ENSO predictability [36]. In terms of the two-parameter bifurcation diagram in Figure 6, linear models would assume that the forcing parameters are from the stable region (below curve TR), and that noise excites the system in the direction of the dominant eigenvectors.

Acknowledgements

References

[1] Henry DI Abarbanel and Matthew B Kennel. Synchronizing high-dimensional chaotic optical ring dynamics. *Phys. Rev. Lett.*, 80(14):3153, 1998.

[2] G Stépán. *Retarded Dynamical Systems*: *Stability and Characteristic Functions*. Longman Scientific and Technical, Harlow, Essex, 1989.

[3] B. Krauskopf. Bifurcation analysis of lasers with delay. In D.M. Kane and K.A. Shore, editors, *Unlocking Dynamical Diversity*: *Optical Feedback Effects on Semiconductor Lasers*, pages 147–183. Wiley, 2005.

[4] H.A. Dijkstra. *Dynamical Oceanography*. Springer-Verlag, New York, 2008.

[5] F.-F. Jin, J.D. Neelin, and M. Ghil. El Niño on the devil's staircase: annual subharmonic steps to chaos. *Science*, 264(5155):70–72, 1994.

[6] F.-F. Jin, J.D. Neelin, and M. Ghil. El Niño/Southern Oscillation and the annual cycle: subharmonic frequency locking and aperiodicity. *Physica D*, 98:442–465, 1996.

[7] E. Tziperman, L. Stone, M.A. Cane, and H. Jarosh. El Niño chaos: Overlapping of resonances between the seasonal cycle and the Pacific ocean-atmosphere oscillator. *Science*, 264:7274, 1994.

[8] J.D. Neelin, D.S. Battisti, A.C. Hirst, F.-F. Jin, Y. Wakata, T. Yamagata, and S.E. Zebiak. ENSO theory. *J. Geophysical Research*, 103(C7):14261–14290, 1998.

[9] E. Tziperman, M.A. Cane, S.E. Zebiak, Y. Xue, and B. Blumenthal. Locking of El Niño's peak time to the end of the calendar year in the delayed oscillator picture of ENSO. *J. Climate*, 11:2191–2199, 1998.

[10] J.K. Hale and S.M. Verduyn Lunel. *Introduction to functional-differential equations*, volume 99 of *Applied Mathematical Sciences*. Springer-Verlag, New York, 1993.

[11] J. Michael T. Thompson and H. B. Stewart. *Nonlinear dynamics and chaos*. Wiley, Chichester, UK, 2 edition, 2002.

[12] J. Guckenheimer and P. Holmes. *Nonlinear oscillations, dynamical systems, and bifurcations of vector fields*, volume 42 of *Applied Mathematical Sciences*. Springer-Verlag, New York, 1990. ISBN 0-387-90819-6.

[13] Y. A Kuznetsov. *Elements of Applied Bifurcation Theory*, volume 112 of *Applied Mathematical Sciences*. Springer-Verlag, New York, third edition, 2004. ISBN 0-387-21906-4.

[14] E. J. Doedel, A. R. Champneys, T. F. Fairgrieve, Y. A. Kuznetsov, B. Sandstede, and X. Wang. *AUTO97, Continuation and bifurcation software for ordinary differential equations*. Concordia University, 1998.

[15] A Dhooge, W Govaerts, and Y A Kuznetsov. MatCont: A Matlab package for numerical bifurcation analysis of ODEs. *ACM Transactions on Mathematical Software*, 29(2):141–164, 2003.

[16] W. Govaerts and Y.A. Kuznetsov. Interactive continuation tools. In B Krauskopf, H M Osinga, and J Galán-Vioque, editors, *Numerical Continuation Methods for Dynamical Systems*: *Path following and boundary value problems*, pages 51–75. Springer-Verlag, Dordrecht, 2007.

[17] B Krauskopf, H M Osinga, and J Galán-Vioque, editors. *Numerical Continuation Methods for Dynamical Systems*: *Path following and boundary value problems*. Springer-Verlag, Dordrecht, 2007.

[18] A.G. Salinger, N.M. Bou-Rabee, R.P. Pawlowski, E.D. Wilkes, E.A. Burroughs, R.B. Lehoueq, and L.A. Romero. *LOCA 1.1 — Library of continuation algorithms*: *Theory and implementation manual*. SANDIA, 2002.

[19] H. A. Dijkstra, F. W. Wubs, A. K. Cliffe, E. Doedel, I. F. Dragomirescu, B. Eckhardt, A. Y. Gelfgat, A. L. Hazel, V. Lucarini, A. G. Salinger, E. T. Phipps, J. Sanchez-Umbria, H. Schuttelaars, L. S. Tuckerman, and U. Thiele. Numerical bifurcation methods and their application to fluid dynamics: analysis beyond simulation. *Commun. Comput. Phys.*, 15:1–45, 2014.

[20] K. Engelborghs, T. Luzyanina, and D. Roose. Numerical bifurcation analysis of delay differential equations using DDE-BIFTOOL. *ACM Transactions on Mathematical Software*, 28(1):1–21, 2002.

[21] R. Szalai, G. Stépán, and S.J. Hogan. Continuation of bifurcations in periodic delay differential equations using characteristic matrices. *SIAM J. Scientific Computing*, 28 (4):1301–1317, 2006.

[22] D. Roose and R. Szalai. Continuation and bifurcation analysis of delay differential equations. In B Krauskopf, H M Osinga, and J Galán-Vioque, editors, *Numerical Continuation Methods for Dynamical Systems*: *Path following and boundary value problems*, pages 51–75. Springer-Verlag, Dordrecht, 2007.

[23] H.A. Dijkstra and M. Ghil. Low-frequency variability of the large-scale ocean circulation: A dynamical systems approach. *Rev. Geophys.*, 43(3):RG3002, 2005.

[24] J. Bjerknes. Atmospheric teleconnections from the equatorial pacific. *Monthly Weather Review*, 97:163–172, 1969.

[25] O. Diekmann, S.A. van Gils, S.M. Verduyn Lunel, and H.-O. Walther. *Delay equations*, volume 110 of *Applied Mathematical Sciences*. Springer-Verlag, New York, 1995.

[26] E J Doedel. Lecture notes on numerical analysis of nonlinear equations. In B Krauskopf, H M Osinga, and J Galán-Vioque, editors, *Numerical Continuation Methods for Dynamical Systems: Path following and boundary value problems*, pages 1–49. Springer-Verlag, Dordrecht, 2007.

[27] J. Sieber and R. Szalai. Characteristic matrices for linear periodic delay differential equations. *SIAM J. Appl. Dynam. Syst.*, 10(1):129–147, 2011.

[28] T. Insperger and G. Stépán. *Semi-Discretization for Time-Delay Systems*. Applied Mathematical Sciences, volume 178. Springer-Verlag, New York, 2011.

[29] T Insperger and G Stépán. Stability chart for the delayed Mathieu equation. *Proc. Roy. Soc. A*, 458(2024):1989–1998, 2002.

[30] V.I. Arnol'd. *Geometrical Methods in the Theory of Ordinary Differential equations*, volume 250 of *Fundamental Principles of Mathematical Sciences*. Springer-Verlag, New York, 1983.

[31] R.P. McGehee and B.B. Peckham. Resonance surfaces for forced oscillators. *Experimental Mathematics*, 3(3):221–244, 1994.

[32] F. Schilder and B. B. Peckham. Computing Arnol'd tongue scenarios. *J. Comput. Phys.*, 220:932–951, 2007.

[33] H. Fazelinia, R. Sipahi, and N. Olgac. Stability robustness analysis of multiple time-delayed systems using building block concept. *IEEE Trans. Automatic Control*, 52(5): 799–810, 2007.

[34] M. Ghil, I. Zaliapin, and B. Coluzzi. Boolean delay equations: a simple way of looking at complex systems. *Physica D*, 237(23):2967 – 2986, 2008.

[35] M. Ghil, M.D. Chekroun, and E. Simonnet. Climate dynamics and fluid dynamics: natural variability and related uncertainties. *Physica D*, 237:2111–2126, 2008.

[36] C. J. Thompson and D. S. Battisti. A linear stochastic dynamical model of ENSO. Part II: Analysis. *J. Climate*, 14:445–466, 2001.

Appendix A. Computation of resonance tongues as surfaces

We now present technical details of how we compute a resonance surface of a DDE of the form (3.1); our method is based on the principle described in [31, 32] for ODEs and has been implemented on top of `DDE-Biftool`.

(i) *Branching off from a resonant torus bifurcation point*

We consider a $k : \ell$ resonant point x on a previously computed torus bifurcation curve in a parameter plane (such as the curve TR in Figure 6), where the periodic orbit Γ undergoing the torus bifurcation has a Floquet multiplier $e^{\pm 2\pi\alpha i}$ with $\alpha = k/\ell$ and $0 < k < \ell$ are coprime integers. We represent this point as the tuple (x, α, η). Here η is assumed to be of dimension two, and the periodic orbit Γ is the solution of the periodic BVP (3.4). Let $z(t)$ be the eigenfunction corresponding to the Floquet multiplier $e^{2\pi i\alpha}$; then z has period ℓ (since k and ℓ do not have a common divisor). We now choose a small radius ρ, and consider as initial guesses for the initial circle (of radius ρ) of locked periodic orbits the family

$$x_{0,\phi}(t) = \Gamma(\ell t) + \rho \cos\phi \operatorname{Re} z(\ell t) + \rho \sin\phi \operatorname{Im} z(\ell t), \quad \phi \in [0, 2\pi/\ell], \quad t \in [0,1],$$

which is parametrised by the angle ϕ. Note that here we have rescaled time again so that $x_{0,\phi}$ has period 1. We now perform a Newton iteration where we keep the two-dimensional system parameter η (initialised to its value at the resonance point) free but fix the integral scalar products

$$0 = \int_0^1 \operatorname{Re} z(\ell t)^T [x_\phi(t) - x_{0,\phi}(t)] \, \mathrm{d}t, \quad 0 = \int_0^1 \operatorname{Im} z(\ell t)^T [x_\phi(t) - x_{0,\phi}(t)] \, \mathrm{d}t. \qquad \text{(A 1)}$$

Together with requiring that x_ϕ satisfies the periodic boundary-value problem (similar to (3.4) but with $T_\Gamma = \ell T_f$)

$$\begin{aligned} \dot{x}_\phi(t) &= \ell T_f f(t, x_\phi(t), x_\phi(t - \tau_1/(\ell T_f)), x_\phi(t - \tau_2/(\ell T_f)), \eta), \\ x_\phi(0) &= x_\phi(1), \end{aligned} \qquad \text{(A 2)}$$

system (A 1)–(A 2) is an equation for the variables (x_ϕ, η) with a locally unique solution for every ϕ and (sufficiently small) initial radius ρ.

(ii) *Branching off from an autonomous periodic orbit*

Creating the initial circle for a resonance surface starting from an autonomous oscillation for zero forcing is slightly different from the case of branching off from a torus curve. Suppose that at $\eta = (\eta_1, \eta_2) = (\eta_1, 0)$ the period T_Γ of a periodic orbit Γ and the forcing period T_f have a ratio k/ℓ, where $0 < k < \ell$ are again coprime; here we assume that the second component η_2 of the parameter η is the amplitude of the forcing. Then we choose as our initial guesses $x_{0,\phi}(t) = x(\ell(t + \phi/(2\pi)))$ (again, rescaling time such that the period of $x_{0,\phi}$ equals 1). Two additional conditions are given by fixing the initial forcing η_2 to the small radius ρ, and by fixing the phase of the initial solution x_ϕ:

$$0 = \int_0^1 \dot{x}_{0,\phi}(t)^T x_\phi(t)\, dt, \quad \eta_2 = \rho. \tag{A 3}$$

Solving (A 2) combined with (A 3) results in an initial topological circle of locked orbits $(x_\phi, (\eta_1, \eta_2))$, parametrised by $\phi \in [0, 2\pi/\ell]$.

(iii) *Growing the surface circle by circle*

Once we have an initial circle of solutions x_ϕ on the resonance surface, we can continue the surface by computing nearby circles (which are generally only topological circles). We parametrise the surface locally by the angle ϕ on the circle and by its orthogonal complement in the tangent space of the solution surface. An equidistributed mesh of solutions on an already computed topological circle is given. We pick a point $(x, \eta)_{\text{old}}$ at angle ϕ on this circle. The tangent space in $(x, \eta)_{\text{old}}$ to the resonance surface is two-dimensional, and can be computed as the two-dimensional nullspace of the linearisation of (A 2) in $(x, \eta)_{\text{old}}$. One component of this tangent space, spanned by $t_1 = (x, \eta)_{\text{tan},1}$, points along the old circle. We denote its orthogonal complement in the tangent space by $t_2 = (x, \eta)_{\text{tan},2}$, and take a small step (of size δ) from $(x, \eta)_{\text{old}}$ along t_2 to obtain an initial guess $(x, \eta)_{\text{new}}$. Newton iteration is used to solve (A 2), augmented with the two linear equations

$$0 = \int_0^1 x_{\text{tan},k}^T [x_\phi(t) - x_{\text{new}}(t)]\, dt + \eta_{\text{tan},k}^T [\eta - \eta_{\text{new}}] \quad \text{for } k = 1, 2. \tag{A 4}$$

This gives for every $\phi \in [0, 2\pi]$ a new solution x_ϕ on the resonance surface. The family of new solutions x_ϕ forms again a topological circle, so that the above procedure can be repeated to 'grow' the resonance surface as a family of topological circles. In practice one has to perform computations only for angles $\phi \in [0, 2\pi/\ell]$, since for any x_ϕ the solution $t \mapsto x_\phi(t - j/\ell)_{\text{mod}[0,1]}$, $j = 1\ldots\ell - 1$, is also a solution.